INSTITUTE OF PHYSICS PUBLISHING PLASMA SOURCES SCIENCE AND TECHNOLOGY
Plasma Sources Sci. Technol. **15** (2006) 773–782 doi:10.1088/0963-0252/15/4/022

Time-varying impedance of the sheath on a probe in an RF plasma

Francis F Chen

Electrical Engineering Department, University of California, Los Angeles, 90095-1594, USA

Received 29 November 2005, in final form 30 November 2005
Published 29 August 2006
Online at stacks.iop.org/PSST/15/773

Abstract
Langmuir probes used in radiofrequency (rf) discharges usually include compensation elements that minimize the effect of high frequency oscillations in plasma potential. The design of these elements requires knowledge of the capacitance of the sheath on the probe tip, a quantity which varies nonlinearly during the rf cycle. Sheath capacitance has been studied previously for capacitively coupled discharges, where the rf is applied to the electrodes. Here the problem is treated from the standpoint of a small probe in a fluctuating discharge. This work differs from existing literature in that (a) no step model is used and the Debye sheath is treated exactly, (b) the treatment is simple and analytic, (c) the time-variation of the capacitance is explicitly shown, (d) the results are applied to probe design and (e) cylindrical geometry is considered. The rf frequency is assumed low enough that electron transit times can be ignored. We find that when the rf excursions bring the sheath from the Child–Langmuir region into the Debye sheath or electron saturation region, its capacitance has a strongly non-linear behaviour.

(Some figures in this article are in colour only in the electronic version)

1. Introduction

In the design of rf-compensated Langmuir probes for measurements in rf plasmas, it is necessary to know the capacitive coupling through the sheath of rf fluctuations in plasma potential. The simple approach normally used is to consider the sheath to be a vacuum capacitor whose thickness is roughly estimated. In plane geometry this thickness is not well defined, even if a sheath edge is well defined, because the thickness depends on the slope of the potential at the edge, and this depends on the transition to the presheath. It is impractical to solve for the presheath, since the solution depends on collisions and ionization and is specific to each discharge. More accurate treatments of rf sheaths can be found in the literature but are not always suitable for the present task.

Lieberman [1,2] has given analytic solutions for the sheath on a driven electrode in a capacitively coupled plasma (CCP). However, he used a model in which the electron density was approximated by a single step. Godyak and Sternberg [3] pointed out that high-and low-frequency approximations can be made depending on whether the rf frequency ω is larger or smaller than the ion plasma frequency Ω_p, and they solved [4] the high-frequency case for a CCP driven symmetrically relative to ground. How the shape of the sheath changes during the rf cycle was computed numerically by Zhang *et al* [5], with the result that large changes occur in the low-frequency case, the one treated in this paper. However, they did not give the sheath capacitance explicitly.

Godyak [3] showed that the sheath capacitance C_{sh} depends only on the surface charge on the probe and can be calculated without solving for the sheath thickness numerically. Sudit and Chen [6] used this shortcut to calculate C_{sh}. In that work, however, they neglected the Debye sheath, treating only the Child–Langmuir (C–L) sheath, adding, rather inconsistently, the Bohm velocity at the sheath edge. Here we solve the plane sheath problem consistently, showing exactly what approximations were previously made and also obtaining formulae from which the sheath capacitance can be calculated even when the probe is not biased far from the space potential. To establish notation, we start with a brief review of plane sheath theory before applying it to the calculation of sheath capacitance as a function of time. Cylindrical sheaths and the resistive part of the sheath impedance will be treated at the end.

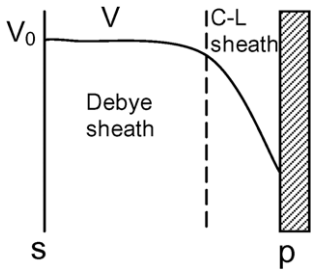

Figure 1. Geometry of a plane sheath.

2. Plane sheaths in a nutshell

2.1. Basic equations

We start by defining a sheath edge s (figure 1) with V_s, n_s and v_s denoting, respectively, the potential, density and ion velocity there. Following traditional practice, we set $V_s = 0$ in the absence of rf and assume quasineutrality up to s so that $n_i(s) = n_e(s) \equiv n_s$. The ions enter the sheath with a unidirectional, monoenergetic velocity v_s, whose Bohm value will be recovered in due course. There is no artificial separation between the Debye sheath (where $n_e \neq 0$) and the Child–Langmuir sheath (where $n_e = 0$). Defining

$$V = \tilde{V} - V_s, \tag{1}$$

where $\tilde{V}$ is the actual potential as V_s varies, we write Poisson's equation as

$$\varepsilon_0 \frac{d^2V}{dx^2} = e(n_e - n_i). \tag{2}$$

For Maxwellian electrons, we have

$$n_e = n_s e^{eV/KT_e}. \tag{3}$$

The ion velocity v is given by energy conservation

$$\frac{1}{2}Mv_s^2 = \frac{1}{2}Mv^2 + eV \,(V \leqslant 0) \tag{4}$$

so that

$$v = \left(v_s^2 - \frac{2eV}{M}\right)^{1/2}. \tag{5}$$

Since ion flux is conserved, we have

$$n_i v_i = n_s v_s, \qquad n_i = n_s v_s / v_i = n_s \left(1 - \frac{2eV}{Mv_s^2}\right)^{-1/2}. \tag{6}$$

The positive, dimensionless potential η is defined as

$$\eta \equiv -e(\tilde{V} - V_s)/KT_e = -eV/KT_e, \tag{7}$$

whereupon Poisson's equation becomes

$$\frac{\varepsilon_0 KT_e}{n_s e^2}\frac{d^2\eta}{dx^2} = \left(1 + \frac{2KT_e}{Mv_s^2}\eta\right)^{-1/2} - e^{-\eta}. \tag{8}$$

Henceforth we use a Roman 'e' for 2.718 and an italic '*e*' for charge. Normalizing x to the Debye length (with $n = n_s$),

$$\lambda_D = (\varepsilon_0 KT_e/n_s e^2)^{1/2}, \qquad \xi \equiv (x - s)/\lambda_D \tag{9}$$

and defining the ion acoustic speed c_s and the Mach number $\mathcal{M}$ as

$$c_s \equiv (KT_e/M)^{1/2}, \qquad \mathcal{M} \equiv v_s/c_s, \tag{10}$$

equation (8) becomes simply

$$\eta'' = \frac{d^2\eta}{d\xi^2} = (1 + 2\eta/\mathcal{M}^2)^{-1/2} - e^{-\eta}. \tag{11}$$

Multiplying by the integrating factor η' and integrating from $\xi = 0$, we obtain

$$\tfrac{1}{2}(\eta')^2 = \mathcal{M}^2[(1 + 2\eta/\mathcal{M}^2)^{1/2} - 1] + [e^{-\eta} - 1]. \tag{12}$$

Here we have used the sheath boundary condition $\eta'(0) = 0$.

2.2. Recovery of the Bohm sheath criterion

Since equation (12) has to be positive for all η, we can get a condition on $\mathcal{M}$ by expanding the rhs for small η, up to order η^2.

$$\tfrac{1}{2}(\eta')^2 = \mathcal{M}^2\left[(1 + \eta/\mathcal{M}^2 - \tfrac{1}{2}\eta^2/\mathcal{M}^4) - 1\right] + \left[1 - \eta + \tfrac{1}{2}\eta^2 - 1\right] = -\tfrac{1}{2}\eta^2/\mathcal{M}^2 + \tfrac{1}{2}\eta^2 \geqslant 0. \tag{13}$$

Hence, $\mathcal{M} \geqslant 1$, or $v_s \geqslant c_s$, which is the Bohm criterion. We can now *define* the 'sheath edge' to be that position s near the wall or probe where this condition is barely satisfied: $v_s = c_s$. Setting $\mathcal{M} = 1$ in equation (12) and taking the square root, we obtain

$$\eta' = \pm\sqrt{2}[(1 + 2\eta)^{1/2} + e^{-\eta} - 2]^{1/2}. \tag{14}$$

This equation differs from previous work on C_{sh} in that the electron density is not neglected or approximated.

2.3. Recovery of the Child–Langmuir law

For space-charge-limited ion emission, the electron terms are omitted, and η is infinitely large, since temperatures are zero. Equation (14) then becomes

$$\eta' = 2^{1/2}(2\eta)^{1/4}, \qquad \eta^{-1/4}\eta' = 2^{3/4}. \tag{15}$$

Integrating from $\xi = 0$ to d/λ_D gives

$$\eta^{3/4} = \frac{3}{4}2^{3/4}\xi_d, \qquad \eta^{3/2} = \frac{9}{16}2^{3/2}\xi_d^2 = \frac{9}{8}2^{1/2}\xi_d^2. \tag{16}$$

Converting back to dimensional units, we have

$$\left(\frac{-eV}{KT_e}\right)^{3/2} = \frac{9}{8}2^{1/2}d^2\left(\frac{n_s e^2}{\varepsilon_0 KT_e}\right). \tag{17}$$

It is now convenient to express n_s in terms of the ion current density J:

$$J = en_s c_s = en_s(KT_e/M)^{1/2}, \qquad n_s = J/e(KT_e/M)^{1/2}. \tag{18}$$

The normalizing factor KT_e now cancels out, as it should, and we have

$$J = \frac{4}{9}\left(\frac{2e}{M}\right)^{1/2}\frac{\varepsilon_0(-V)^{3/2}}{d^2}, \tag{19}$$

which is exactly the Child–Langmuir law.

2.4. Relation to the plasma potential

Since the ions have a velocity c_s at s, they must have gained an energy $\frac{1}{2}Mc_s^2 = \frac{1}{2}KT_e$ in the presheath, so that the potential V_0 in the main plasma must be higher than V_s by $\frac{1}{2}KT_e/e$. The electrons, if Maxwellian, would have a density higher by a factor $e^{1/2}$ in the plasma than at the sheath edge. Thus, $n_s = e^{-1/2}n_0 = 0.61n_0$. Since λ_D was defined with $n_s^{-1/2}$, its value would be decreased by $e^{-1/4} = 0.78$ if we had chosen to define it using n_0. The derivative η' would be increased by a factor $e^{1/4} = 1.28$. However, once this is understood, it is not necessary to make any changes in the formulism.

3. Calculation of sheath capacitance

The charge on a capacitor is given by $Q = CV$. From this, the sheath capacitance C_{sh} can be written as

$$\frac{C_{sh}}{A_p} = \frac{\Delta\rho_s}{\Delta V}, \tag{20}$$

where A_p is the probe area and ρ_s is the surface charge density on the probe. Following [6], we use Gauss's Law to obtain $\rho_s = D_n$, the normal component of $\varepsilon_0 E = -\varepsilon_0(-\nabla V)$. The first minus sign comes from the fact that D_n is defined in the $-x$ direction in figure 1. Equation (20) then becomes

$$\frac{C_{sh}}{A_p} = -\varepsilon_0\frac{\Delta E}{\Delta V} = \varepsilon_0\frac{d}{dV}\left(\frac{dV}{dx}\right) = \frac{\varepsilon_0}{\lambda_D}\frac{d}{d\eta}\left(\frac{d\eta}{d\xi}\right). \tag{21}$$

Equation (14) gives $d\eta/d\xi$. Taking its η-derivative, we obtain

$$\frac{C_{sh}}{A_p} = \frac{\varepsilon_0}{\lambda_D}\frac{1}{\sqrt{2}}\frac{(1+2\eta)^{\frac{1}{2}} - e^{-\eta}}{[(1+2\eta)^{\frac{1}{2}} + e^{-\eta} - 2]^{1/2}}, \tag{22}$$

where we have taken the + sign because the ion density (the first term in the numerator) has to be larger than the electron density (the second term) once the Bohm criterion is satisfied. Here it is understood that η is evaluated at the probe, so that $\eta = -e(V_p - V_s)/KT_e$. This equation is valid for all V_p below the space potential even if η is small.

The error in neglecting the Debye sheath [6] can now be calculated. If we neglect $e^{-\eta}$ and its integration constant, the fraction F in equation (22) becomes

$$F = (1+2\eta)^{-\frac{1}{2}}[(1+2\eta)^{\frac{1}{2}} - 1]^{-\frac{1}{2}} = [(1+2\eta)^{3/2} - (1+2\eta)]^{-\frac{1}{2}}. \tag{23}$$

This can be expanded in the small quantity $\varepsilon \equiv 1/(2\eta)$ to obtain

$$F = \varepsilon^{3/4}\left(1 - \varepsilon^{1/2} + \frac{3}{2}\varepsilon - \cdots\right)^{-1/2} \approx \varepsilon^{3/4}\left(1 + \frac{1}{2}\varepsilon^{1/2} - \frac{3}{4}\varepsilon + \cdots\right). \tag{24}$$

Thus the capacitance is approximately

$$\frac{C_{sh}}{A_p} = \frac{\varepsilon_0}{\lambda_D}\frac{(2\eta)^{-3/4}}{2^{\frac{1}{2}}}\left(1 + \frac{1}{2}\frac{1}{(2\eta)^{\frac{1}{2}}}\right). \tag{25}$$

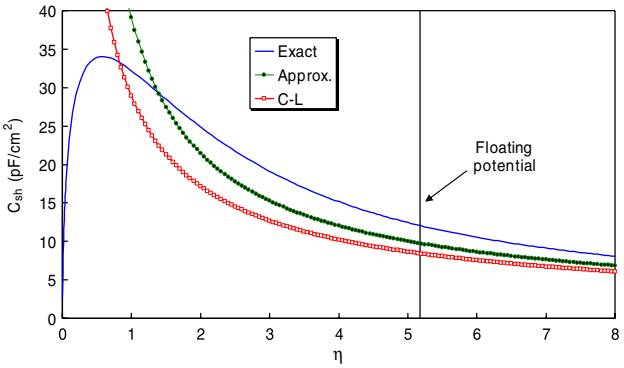

Figure 2. Sheath capacitance versus normalized probe bias according to the exact formula (——), its Taylor expansion (●) and the Child–Langmuir formula (○).

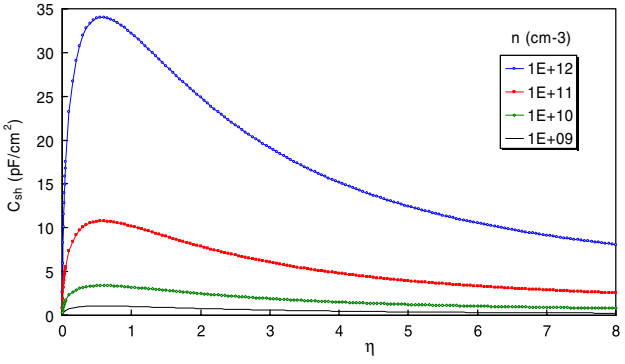

Figure 3. Variation of dc C_{sh} with density.

Apart from notation, this is the same as equation (17) of [6] if one approximates n_s with $\frac{1}{2}n_0$ (section 2.4). The correction term in equation (25), which modifies the Child–Langmuir sheath for the incident ion velocity, is not small. At the floating potential, η is about 5, so that term is ≈0.16. For smaller η (V_p closer to space potential) the expansion fails, and one should use the exact equation (22), which includes the Debye sheath. Physically, equation (25) tells us that the sheath capacitance increases as η decreases—that is, as the sheath gets thinner—more or less as predicted by the Child–Langmuir law. There is, in addition, a dependence on T_e and n_0 through λ_D.

Figure 2 shows computations of C_{sh} versus η comparing the exact formula of equation (22) with the approximate formulae of equations (25) and (28). At large η, all the curves show a decrease in C_{sh} with η as the C–L sheath thickness increases. The exact curve shows a peak at small η as the probe enters the Debye sheath, and it falls at smaller η as the thickness of the Debye sheath increases to ∞ as V_p reaches the space potential. Approximations that do not include the Debye sheath do not have this feature. The approximation (25) that includes the ion velocity at the sheath edge is somewhat better than the C–L approximation (28), which does not. The improvement is not great, since the series in equation (24) converges very slowly with $\eta^{\frac{1}{2}}$. At the floating potential either approximation is reasonably good, but they fail when the V_p moves closer to V_s. Figure 3 shows the expected variation of C_{sh} with density.

4. Effect of RF

4.1. Range of validity

In rf discharges, an electric field is applied to the plasma either by an electrode or by an external antenna. This E-field can drive electrons towards a wall. The sheath drop there must then increase to repel enough electrons to maintain a neutral plasma, and the plasma potential V_0 must rise. As the rf changes sign, V_0 will rise and fall unsymmetrically, since the current through a Coulomb barrier varies exponentially with voltage. The harmonic content of V_0 oscillations will vary in different devices. Godyak and Piejak [7] showed that the 2nd harmonic will dominate in a CCP with electrodes driven symmetrically relative to ground [4]. In a normal CCP with one electrode near ground, the fundamental rf frequency ω will dominate. In a cylindrical inductively coupled plasma (ICP), the E-field is ideally everywhere parallel to the walls so that no oscillating wall sheaths develop, but asymmetries in antenna construction, ports on the walls and capacitive coupling can cause V_0 oscillations at the fundamental frequency ω. In helicon discharges, an E-field at ω is an intrinsic property of the helicon wave. To simplify the problem, we will treat one frequency at a time and assume that V_s, the sheath-edge potential, follows the oscillations in V_0.

The dc sheath theory given above is applicable only if the sheath comes into equilibrium at each phase of the rf. This requires, first, that the rf frequency f_{rf} be low enough that the electrons respond instantaneously; this is a good assumption. Second, the frequency must be low enough that the ions traverse the sheath before it changes, and their rf motion need not be taken into account [3,5]. If the sheath thickness is about $5\lambda_D$, the ion transit time t through the sheath is

$$t \approx 5\lambda_D/c_s \approx 5\left(\frac{\varepsilon_0 KT_e}{n_0 e^2}\right)^{1/2}\left(\frac{M}{KT_e}\right)^{1/2} = \frac{5}{\Omega_p}, \qquad (26)$$

Ω_p being the ion plasma frequency. The rf period $\tau = 1/f_{rf} =$ must then be $\gg 2t$, yielding

$$f_{rf} \ll \Omega_p/10. \qquad (27)$$

At $n_0 = 10^{12}\,\mathrm{cm}^{-3}$, Ω_p is $\approx 2 \times 10^8\,\mathrm{s}^{-1}$, so that f_{rf} must be $\ll 20\,\mathrm{MHz}$. This is marginally acceptable at 13.56 MHz, and the condition is not met at lower densities even at that frequency. Fortunately, the value of C_{sh} need not be known exactly in practical applications.

This being the case, we may use equation (25) without the correction term; the error entailed was discussed in section 3. In dimensional units, this is

$$C_{sh} = \frac{A_p}{2^{5/4}}\frac{\varepsilon_0}{\lambda_D}\left[\frac{e(V_s - V_p)}{KT_e}\right]^{-3/4}. \qquad (28)$$

In the absence of rf, the capacitance is [6]

$$C_0 = \frac{A_p}{2^{5/4}}\frac{\varepsilon_0}{\lambda_D}\left[\frac{e(\bar{V}_s - \bar{V}_p)}{KT_e}\right]^{-3/4}, \qquad (29)$$

where the overbar denotes the dc values.

4.2. Uncompensated probe

4.2.1. Small rf fluctuations. In the presence of rf, consider first a probe or small electrode connected directly to a dc power supply, giving $V_p = \bar{V}_p$. Let V_s oscillate at frequency ω:

$$V_s = \bar{V}_s + V_{rf}\sin\omega t. \qquad (30)$$

The capacitance is then given by

$$C_{sh} = C_0\left(1 + \frac{V_{rf}\sin\omega t}{\bar{V}_s - \bar{V}_p}\right)^{-3/4}. \qquad (31)$$

In addition to C_{sh} changing with probe voltage, it also changes during an rf cycle. If V_{rf} is small, equation (31) can be expanded and averaged over an rf cycle. We then find that $\langle C_{sh}\rangle$ differs from C_0 only in second order in $V_{rf}/(\bar{V}_s - \bar{V}_p)$.

4.2.2. Large rf fluctuations. A more likely situation, however, is that V_{rf} is larger than $\bar{V}_s - \bar{V}_p$, which can be as small as $2KT_e/e$ as the probe I–V curve is swept, while V_{rf} can exceed 100 V. In that case, equation (31) shows that C_{sh} has a pole and becomes complex when the bracketed quantity goes negative. This cannot happen physically, however. When V_s comes close to V_p, the probe draws a large electron current, raising the mean plasma potential $\bar{V}_s$. Thus, $\bar{V}_s$ has to increase, keeping the bracket positive. Since $\bar{V}_s$ is no longer constant and the approximation $\eta \gg 1$ is not always valid, we must use the exact equation (22):

$$\frac{C_{sh}}{A_p} = \frac{\varepsilon_0}{\lambda_D}\frac{1}{\sqrt{2}}\frac{(1+2\eta)^{-\frac{1}{2}} - \mathrm{e}^{-\eta}}{\left[(1+2\eta)^{\frac{1}{2}} + \mathrm{e}^{-\eta} - 2\right]^{1/2}}. \qquad (32)$$

Under normal circumstances, η is always positive if the probe is biased below V_s. The denominator is positive if the Bohm criterion is satisfied (section 2.2), and the numerator is always positive since its leading term in a Taylor expansion is η^2. Recall that η is defined as

$$\eta = \frac{e}{KT_e}\left[V_{rf}\sin\omega t + (\bar{V}_s - \bar{V}_p)\right]. \qquad (33)$$

If $\sin\omega t$ is positive or only slightly negative so that η remains positive, electron saturation is never reached, and equation (32) is still correct. For more negative values of $\sin\omega t$, η would become negative unless $\bar{V}_s$ increases. The amount of this increase depends on the geometry. To keep the plasma neutral, the electron flux to the probe cannot exceed the ion flux to the walls. For simplicity, we neglect the ion flux to the probe and the electron flux to the walls. The electron flux to the probe is

$$J_e = A_p n_0 v_r \mathrm{e}^{-\eta} \quad (\eta \geqslant 0), \qquad v_r = (KT_e/2\pi m)^{\frac{1}{2}}, \qquad (34)$$

where v_r is the electrons' random thermal velocity. The ion flux to the walls of area A_w is

$$J_i = A_w n_s c_s = A_w \mathrm{e}^{-\frac{1}{2}} n_0 (KT_e/M)^{\frac{1}{2}}. \qquad (35)$$

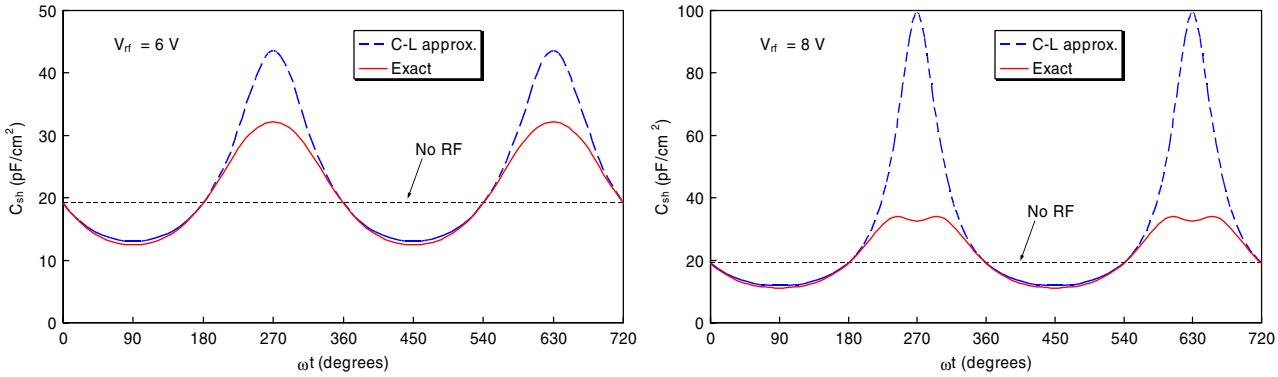

Figure 4. Variation of C_{sh} through two rf cycles for $V_{rf} = 6$ and 8 V (0-to-peak). The solid curve (——) is the exact solution and the dashed curve (- - - -) the C–L approximation. Parameters are $n = 10^{12}$ cm^{-3}, $KT_e = 3$ eV and $\eta_{dc} = 3$.

The minimum value of η is thus given by equating these two fluxes:

$$e^{\eta_{min}} = \frac{A_p n_0 v_r}{A_w n_s c_s} = \frac{A_p}{A_w}\left(\frac{e}{2\pi}\frac{KT_e}{m}\frac{M}{KT_e}\right)^{1/2}, \qquad (36)$$

$$\eta_{min} = \frac{1}{2}\left[1 + \ln\left(\frac{M}{2\pi m}\frac{A_p^2}{A_w^2}\right)\right]. \qquad (37)$$

Note that 'e' here is *not* the unit charge 'e'. From equation (33), $\bar{V}_s$ must rise to the value

$$\bar{V}_s = \bar{V}_p - V_{rf}\sin\omega t - (KT_e/e)\eta_{min}. \qquad (38)$$

For rf phases such that $\sin\omega t$ is negative and large enough that $\eta < \eta_{min}$ in equation (33), the sheath capacitance is given by equation (32) with η replaced by η_{min}. Thus, for large V_{rf}, C_{sh} obeys equation (32) for only part of the rf cycle. When $\sin\omega t$ swings sufficiently negative, $\bar{V}_s$ rises to keep the plasma neutral, and C_{sh} remains constant during that part of the rf cycle.

Note, however, that equation (34) is valid only for $\eta \geqslant 0$. Electron saturation is reached at $\eta = 0$, and J_e remains at the value $A_p n_0 v_r$. That means that η_{min} must be non-negative and the argument of the logarithm in equation (37) must be $>1/e$. If the probe area is so small that it can draw saturation electron current without raising V_s, then the sheath vanishes, having infinite thickness. Indeed, if we replace η by $\eta_{min} = 0$ in equation (32), we find that C_{sh} has the indeterminate form 0/0, which can be seen to approach 0 by taking the derivatives of the numerator and denominator.

In summary, we see that C_{sh} varies in a very complicated way in the presence of V_{rf}. There are four cases. (i) If V_{rf} is so small that V_s never oscillates below $\bar{V}_p$, C_{sh} is affected only in higher order. (ii) For larger V_{rf}, C_{sh} will vary nonsinusoidally with the phase of the rf. (iii) If V_{rf} is very large, $\bar{V}_s$ will be changed by the probe current so as to keep η positive, and C_{sh} will reach a limiting value during part of the rf cycle. (iv) If the probe is very small, η_{min} itself will saturate at the value 0. These cases are illustrated in figures 4–6. Figure 4 compares C_{sh} computed using equation (32) with that using equation (31). At $V_{rf} = 6$ V, the excursions are small enough that η does not enter the region to the left of the peak in figure 2 and is near the limit of case (i) . At $V_{rf} = 8$ V, that region is entered when $\sin\omega t \approx -1$, and the exact solution shows a dip in C_{sh}. This dip reaches 0 at $V_{rf} = 9$ V, since $e(V_s - V_p)$ starts at $3\ KT_e = 9$ V, and V_{rf} is just sufficient to bring V_s down to V_p at its extremum. This is case (ii).

Figure 5 shows case (iii), when η is limited by η_{min}, but η_{min} is still above the dc value of $\eta = 3$. The 'exact' solution of equation (32) is compared with that when the η_{min} cutoff is imposed by the fact that V_s is dragged upwards by the probe current. This rare case happens only when the plasma chamber is small, so that the ratio A_w/A_p in equation (37) is not very large. However, we have observed experimentally that the shift in $\bar{V}_s$ is larger than expected from the calculation above, so that case (iii) may occur for larger values of A_w/A_p.

Figure 6 shows case (iv) when A_w/A_p has a more normal value of 2800/0.047 (an 0.015 × 1 cm diam probe in a 30 cm diam × 30 cm high chamber). In this case, the large V_s oscillations quickly bring V_s down to V_p whenever $\sin\omega t$ is negative, and $\eta_{min} \to 0$ for a large portion of the rf period. C_{sh} also goes to 0, corresponding to the left edge of the exact curve in figure 2. The only difference between the curves is that the 'exact' equation (32) has no solution for $\eta < 0$, while 'cutoff' solution replaces η with $\eta_{min} = 0$.

The sudden jumps in C_{sh} would give rise to high harmonics in the probe current. These jumps are an artefact of the plane-geometry idealization. In cylindrical geometry the electron current does not saturate abruptly but slowly grows as the electron sheath expands. The curves in figure 6 should be smoothed out, but we shall see in section 5 that the situation is not simple. In the next two sections, we examine methods devised to avoid the complicated behaviour of C_{sh} by limiting the effective V_{rf} to small values.

4.3. Partially compensated probe

The most common way to deal with rf fluctuations in V_0 is to use tuned inductors and auxiliary floating electrodes, a method tried by Gagne and Cantin [8, 9] and further developed by Godyak *et al* [10], Sudit and Chen [6] and Mahony *et al* [11]. A partially compensated probe is shown in figure 7. The probe tip is located at P. The sheath capacitance C_{sh} connects it to the space potential V_s. A choke chain with impedance Z_{ck} consisting of inductors and their stray capacitances filters out the rf fluctuations $\tilde{V}_s$ from the resistor R_m across which the probe current is measured. The value of R_m is small and can be neglected in this discussion. Ideally, the probe tip then

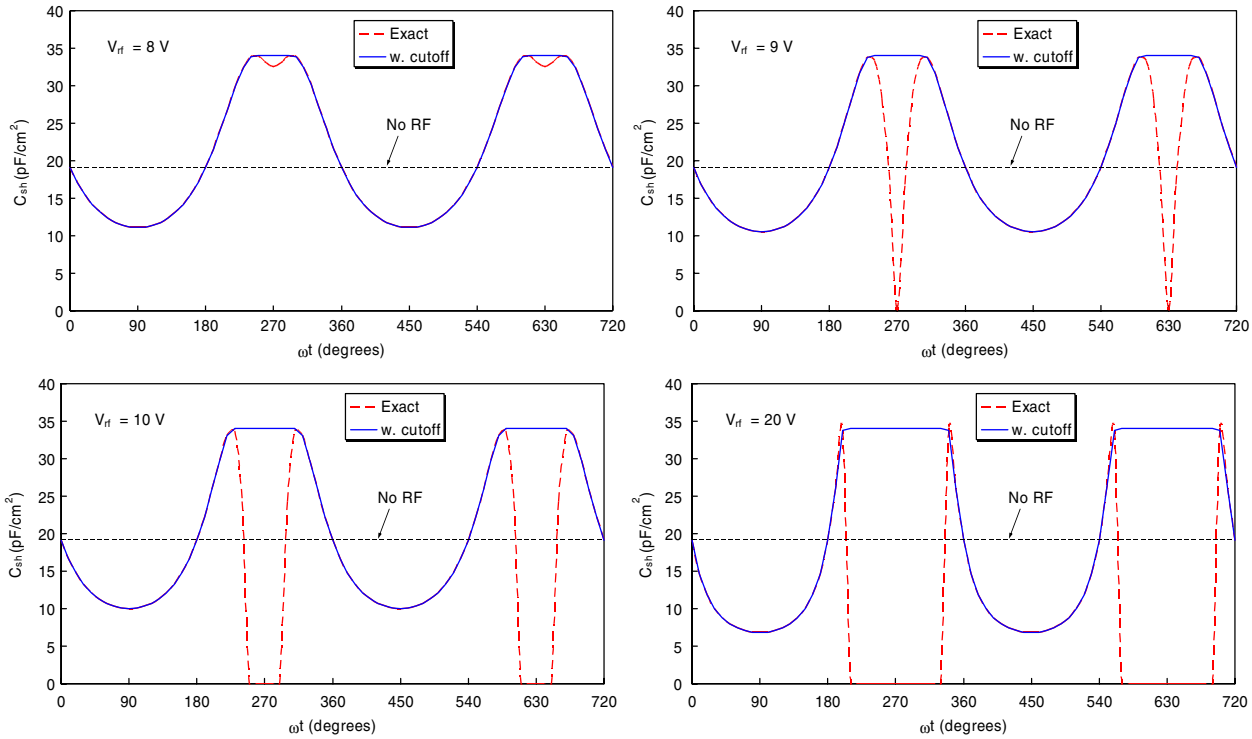

Figure 5. Comparison of the 'exact' solution (- - - -) with that imposed by $\eta_{\min}$ as $V_{\rm rf}$ is increased (——). The $V_{\rm rf} = 8$ V case is the same as in figure 4. The ratio $A_{\rm w}/A_{\rm p}$ is only 100 here.

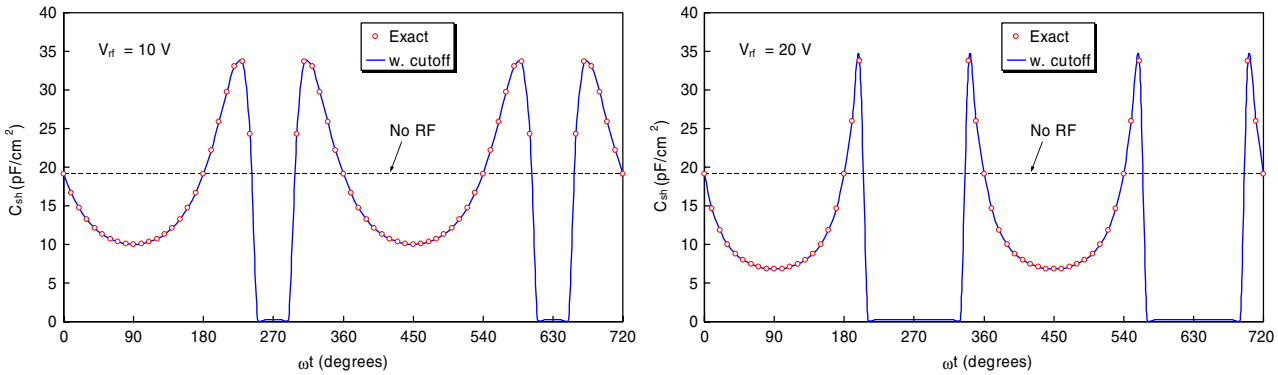

Figure 6. Behaviour of $C_{\rm sh}$ for small probes and large $V_{\rm rf}$. The 'exact' solution (○) does not exist where the 'cutoff' solution (——) gives $C_{\rm sh} = 0$.

fluctuates with $\tilde{V}_{\rm s}$ so that the applied dc voltage $V_{\rm p}$ is the only voltage between the probe and the plasma. Ignoring the stray capacitance $C_{\rm s}$ for the moment, we see that $C_{\rm sh}$ and $Z_{\rm ck}$ form a voltage divider, and the rf signal at P is

$$\tilde{V}_{\rm p} = \tilde{V}_{\rm s}\frac{Z_{\rm ck}}{Z_{\rm ck} + Z_{\rm sh}}, \tag{39}$$

where $Z_{\rm sh}$ is $-j/\omega C_{\rm sh}$. To suppress rf pickup, therefore, $|Z_{\rm ck}|$ must be much larger than $|Z_{\rm sh}|$ so that $\tilde{V}_{\rm p}$ follows $\tilde{V}_{\rm s}$ closely. To get probe I–V characteristics unaffected by $\tilde{V}_{\rm s}$ requires

$$\eta_{\rm rf} = (e/KT_{\rm e})(\tilde{V}_{\rm s} - \tilde{V}_{\rm p}) \ll 1, \tag{40}$$

where

$$\eta = \eta_{\rm dc} + \eta_{\rm rf} = (e/KT_{\rm e})(\bar{V}_{\rm s} + \tilde{V}_{\rm s} - \bar{V}_{\rm p} - \tilde{V}_{\rm p}). \tag{41}$$

From equation (39) with $\tilde{V}_{\rm s} \approx \tilde{V}_{\rm rf}$, the requirement is [7]

$$\frac{e\tilde{V}_{\rm rf}}{KT_{\rm e}}\left|\frac{Z_{\rm sh}}{Z_{\rm ck} + Z_{\rm sh}}\right| \approx \frac{e\tilde{V}_{\rm rf}}{KT_{\rm e}}\left|\frac{Z_{\rm sh}}{Z_{\rm ck}}\right| \ll 1. \tag{42}$$

To get an order of magnitude, we can use equation (29) to estimate $C_{\rm sh}$. For typical parameters $A_{\rm p} = 0.047\,{\rm cm}^2$ (0.15 mm diam × 1 cm long), $KT_{\rm e} = 3\,{\rm eV}$, $n = 10^{12}\,{\rm cm}^{-3}$, this gives $C_0 = 42\,{\rm pF}$ and $|Z_{\rm sh}| = 280\Omega$ at 13.56 MHz. Here we have assumed $\bar{V}_{\rm p}$ near floating potential, so that $\bar{V}_{\rm p} - \bar{V}_{\rm s} \approx 5$. If $\tilde{V}_{\rm rf} = 100$ V, we would require $|Z_{\rm ck}| \gg 10\,{\rm k}\Omega$, or $|Z_{\rm ck}| \geqslant 100\,{\rm k}\Omega$. At lower densities, this value increases as $n^{-\frac{1}{2}}$. To get an impedance this high usually requires using tuned chokes whose self-resonance is at the rf frequency.

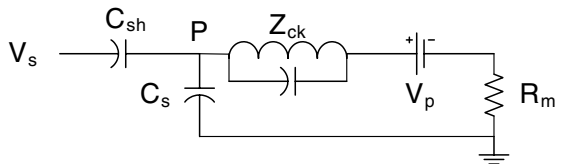

Figure 7. Isolation of a probe with a choke.

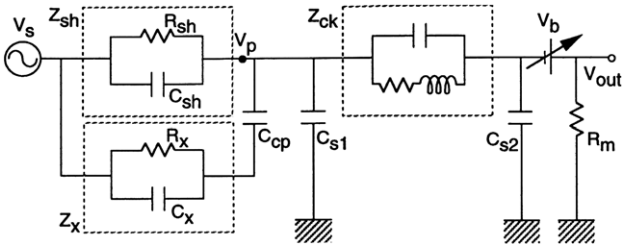

Figure 8. (from [1]).

4.4. Fully compensated probe

A choke chain alone, however, is insufficient because of the stray capacitance C_s of the short wire between the probe tip and the choke chain [6,7]. If C_s connects P to ground, it effectively decreases the value of $|Z_{sh}|$. If C_s connects P to the plasma through a ceramic probe insulator, it has little effect, since it simply adds a small amount to C_{sh}. If $\tilde{V}_s$ varies in space, there may be a small difference between the $\tilde{V}_s$ sampled by C_s and that seen by the probe tip, but this cannot be a large effect.

However, in a real situation, it was found [6] that $|Z_c| \approx 200\,\mathrm{k}\Omega$ gave insufficient rf isolation even if a metal probe shaft was not used. In this case, an auxiliary electrode or 'compensation electrode' of large area A_x (and hence large C_x) is required to detect the rf changes in V_0. Figure 8 shows the probe circuit with both sheaths included [6]. Here C_{sh} is on the probe tip and C_x is on the auxiliary electrode. The latter is coupled to the probe through the relatively large capacitor C_{cp}. C_x is given by equations (32) and (33) but with a larger area A_x, large enough to satisfy equation (42) even if Z_{ck} is bypassed by the stray capacitance C_{s1}.

As far as the probe is concerned, $\tilde{V}_p$ is driven by the compensation electrode and is given by equation (39) with Z_x in place of Z_{sh}:

$$\tilde{V}_p = \tilde{V}_s \left| \frac{Z_{ck}}{Z_{ck} + Z_x} \right|. \tag{43}$$

The requirement of equation (42) is then relaxed to

$$\frac{e\tilde{V}_{rf}}{KT_e} \left| \frac{Z_x}{Z_{ck} + Z_x} \right| \approx \frac{e\tilde{V}_{rf}}{KT_e} \left| \frac{Z_x}{Z_{ck}} \right| \ll 1, \tag{44}$$

and $|Z_{ck}|$ can be smaller by the ratio A_x/A_p. If A_x is large enough, it may not be necessary to use resonant chokes. For instance, if $A_p \approx .05\,\mathrm{cm}^2$, and $A_x \approx 5\,\mathrm{cm}^2$ (0.5 cm diam $\times$ 3 cm long), $|Z_{ck}|$ can be reduced a factor 100 below the $100\,\mathrm{k}\Omega$ calculated in the previous example. However, note that C_{sh} depends on $1/\lambda_D \propto \sqrt{n}$. If $n \approx 10^9\,\mathrm{cm}^{-3}$ instead of $10^{12}\,\mathrm{cm}^{-3}$, $|Z_{sh}|$ is increased by a factor of 32, and $|Z_{ck}|$ of order $30\,\mathrm{k}\Omega$ is still required.

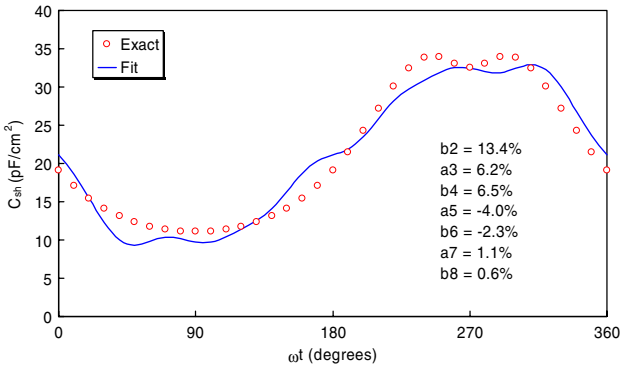

Figure 9. A Fourier fit to the exact curve of figure 4 for $V_{rf} = 8$ V. The harmonic amplitudes relative to the fundamental are shown.

4.5. Generation of harmonics

Since C_{sh} varies with V_s, the rf probe current will be non-sinusoidal, and harmonics of the rf frequency will be generated. To estimate this, we use the approximate formula (31):

$$C_{sh} = C_0 \left(1 + \frac{V_{rf} \sin \omega t}{\bar{V}_s - \bar{V}_p} \right). \tag{45}$$

The ac electron current to the probe is given by

$$\tilde{I}_e = C_{sh}(\mathrm{d}V_s/\mathrm{d}t). \tag{46}$$

From equations (30) and (45), we obtain

$$\tilde{I}_e = C_0 \left(1 + \frac{V_{rf} \sin \omega t}{\bar{V}_s - \bar{V}_p} \right)^{-3/4} (V_{rf}\omega \cos \omega t). \tag{47}$$

For sufficiently small V_{rf}, Taylor expansion gives

$$\begin{aligned} \tilde{I}_e &= C_0 \left(1 - \frac{3}{4} \frac{V_{rf} \sin \omega t}{\bar{V}_s - \bar{V}_p} \right) (V_{rf}\omega \cos \omega t) \\ &= \omega C_0 V_{rf} \left(\cos \omega t - \frac{3}{8} \frac{V_{rf} \sin 2\omega t}{\bar{V}_s - \bar{V}_p} \right). \end{aligned} \tag{48}$$

When the expansion is valid, the 2nd harmonic is smaller than the fundamental by a factor [6]

$$\frac{3}{8} \frac{V_{rf}}{\bar{V}_s - \bar{V}_p}. \tag{49}$$

This is, of course, valid only for very small values of V_{rf}. To see the effect of a more exact calculation, we have Fourier analysed the fairly smooth curve of figure 4(*b*), representing a V_{rf} of only 8 V. The Fourier fit up to the 8th harmonic is shown in figure 9. The non-zero coefficients a_n of $\sin(n\omega t)$ and b_n of $\cos(n\omega t)$ are given relative to that of the fundamental, a_1. The largest harmonic, the 2nd, has 13% amplitude in this case. The leading term in $\tilde{I}_e$ is still given by equation (48).

4.6. The sheath resistance

The real part of Z_{sh} , corresponding to the particle current to the probe, is also nonlinear. We consider only the electron current, since the ion current is comparatively constant and is

not greatly changed by fluctuations in V_s. For a Maxwellian distribution the electron current is given by equation (34):

$$I_e = -eA_p n_0 v_r e^{e(V_s - V_p)/KT_e}. \tag{50}$$

The sheath resistance is defined by

$$R_{sh} = dV/dI, \tag{51}$$

so that, in the absence of rf, the dc resistance is given by

$$R_{sh}^{-1} = dI_e/d(V_p) = (e/KT_e)|I_e|, \tag{52}$$

with $V_s = \bar{V}_s =$ constant. At the floating potential, $|I_e|$ is equal to I_i, and R_{sh} there is given by

$$R_{sh}(V_f) = \frac{KT_e}{e}\frac{1}{eI_i} = \frac{KT_e}{e^2}\frac{1}{n_s c_s A_p}$$
$$= \frac{KT_e}{e^2}\frac{1}{e^{-\frac{1}{2}} n_0 c_s A_p} = \frac{(eMKT_e)^{\frac{1}{2}}}{A_p n_0 e^2}. \tag{53}$$

Note that the 'e' not in italics is not the unit charge. As the probe bias $\bar{V}_p$ increases, $|I_e|$ increases, and R_{sh} decreases from this value exponentially.

In the presence of rf, V_s will oscillate and be given by $V_s = \bar{V}_s + V_{rf}\sin\omega t$. If the probe is uncompensated, V_p will remain at V_p. The I–V curve will oscillate horizontally, and its slope will change, causing R_{sh} to change nonlinearly during the rf cycle. Its value is still given by equations (52) and (50) if V_s is given its unsteady value. If the probe is rf compensated, as subsection 4.4, V_p will follow V_s, and the slope of the I–V curve will not change as much. R_{sh} is still given by equations (52) and (50) if $V_s - V_p$ is given its compensated value. From equation (43) we obtain

$$\tilde{V}_s - \tilde{V}_p = V_{rf}\sin\omega t \left|\frac{Z_x}{Z_{ch} + Z_x}\right|. \tag{54}$$

The instantaneous sheath resistance from equations (52), (50) and (54) can now be written as

$$R_{sh} = \frac{KT_e}{e}\frac{e^{-\left[\bar{V}_s - \bar{V}_p + \frac{e}{KT_e}\left|\frac{Z_x}{Z_{ch}+Z_x}\right| V_{rf}\sin\omega t\right]}}{eA_p n_0 v_r}. \tag{55}$$

The same proviso on negative values of $\sin\omega t$ that makes the exponent positive applies here, but with good compensation this should not happen. The dynamic impedance of a plane sheath in a strong rf environment is then given by

$$Z_{sh} = R_{ch} - j/\omega C_{sh}, \tag{56}$$

in which the resistive and reactive elements have been treated in detail above.

5. Cylindrical geometry

A compensation electrode is usually large enough compared with λ_D that the sheath on it can be treated as planar. A wire probe tip, however, is likely to be made with radius R_p smaller than or comparable to λ_D in order for the orbital-motion-limited (OML) probe theory to be applicable. In that case, the probe sheath has to be treated in cylindrical geometry. In the electron retardation region, Poisson's equation (11) is replaced by the cylindrical version [12] of the Allen–Boyd–Reynolds [13] (ABR) equation

$$\frac{1}{\rho}\frac{d}{d\rho}\left(\rho\frac{d\eta}{d\rho}\right) = \frac{J}{\rho}\eta^{-\frac{1}{2}} - e^{-\eta}, \qquad J \equiv \frac{1}{2\pi\sqrt{2}}\frac{I_i}{en_0}\frac{1}{\lambda_D c_s}, \tag{57}$$

where $\rho = r/\lambda_D$. This equation is not amenable to an analytic solution suitable for probe design. It has to be integrated from infinity, and it does not make sense [14] to define a sheath edge where $v_i = c_s$. Furthermore, the ion current I_i has to be assumed at the outset.

Although we cannot easily extend the plane results for the retardation region to cylinders, we can treat the region of electron saturation. When $V_p > V_s$ so that $\eta < 0$, electrons are accelerated towards the probe. Their thermal velocities will cause those with high angular momentum to orbit the probe and miss it; they cannot be treated as a cold fluid, as we did with the ions. The equations have been solved numerically by Laframboise [15], but these specific results cannot be applied to the general case. However, if R_p/λ_D is small enough, it is possible to use the convenient OML theory of Mott-Smith and Langmuir [16], as summarized by Chen [17]. The orbits of particles spiralling in to an attractive probe are calculated using energy and momentum conservation as in subsection 2.1, but in the case of electrons one cannot neglect their energy spread at the sheath edge. For a Maxwellian distribution at $r = s$, the OML result for saturation electron current is

$$I_{e,sat} = A_p e n_0 v_r F, \tag{58}$$

where v_r is given by equation (34) and F is the function

$$F \equiv \frac{1}{\varepsilon}\mathrm{erf}(\Phi^{\frac{1}{2}}) + e^{-\eta}[1 - \mathrm{erf}(\Phi - \eta)^{\frac{1}{2}}], \tag{59}$$

in which

$$\varepsilon \equiv R_p/s \quad < 1\,, \quad \Phi \equiv \eta/(1 - \varepsilon^{-2}),$$
$$\Phi - \eta = \eta/(\varepsilon^2 - 1). \tag{60}$$

Here η is still defined by equation (7) and is negative for $V_p > V_s$, so that the arguments of the error functions

$$\mathrm{erf}(x) \equiv \int_0^x e^{-t^2} dt \to [x \to 0]\frac{2x}{\sqrt{\pi}} \tag{61}$$

are real. The sheath radius s has to be arbitrarily assumed, since there is no Bohm criterion for electrons when $T_e > T_i$. However, it turns out that F is extremely insensitive to ε for all $\varepsilon > 10$, a fact that Langmuir could not point out because he did not have personal computers. We may therefore take the $s \to \infty$ limit of equation (59), obtaining

$$F(\eta) = \frac{2}{\sqrt{\pi}}(-\eta)^{\frac{1}{2}} + e^{-\eta}[1 - \mathrm{erf}(-\eta)^{\frac{1}{2}}]. \tag{62}$$

Note that at the space potential $\eta = 0$, $F \to 1$ and $F'(\eta) \to -1$, so that $I_{e,sat}$ joins smoothly onto the transition region (equation (34)). An ideal OML probe curve is shown in figure 10. At $V_s = 0$, the junction at V_s is smooth for a cylindrical probe but abrupt for a plane probe. As V_{rf} oscillates with amplitude 6 V, the probe bias V_p effectively oscillates relative to this curve between the limits shown. In this case, V_{rf} is large enough that the probe enters the electron saturation

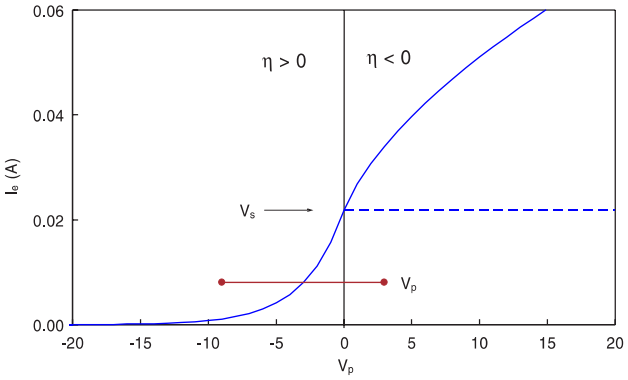

Figure 10. An ideal OML curve for a cylindrical probe with $R_p = 0.0075$ and $L = 1$ cm. The argon plasma has $KT_e = 3$ eV and $n = 10^{11}$ cm^{-3}. The dashed line is the saturation electron current for a plane probe. The effective excursion of V_p is shown for $V_{rf} = 6$ V and $\eta_0 = 1$.

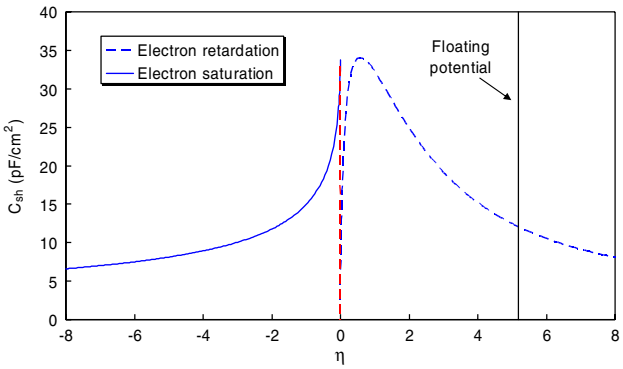

Figure 11. Behaviour of C_{sh} of a cylindrical electron sheath (——); the magnitude is approximate. Also shown for comparison is C_{sh} for a plane ion sheath (- - - -) from figure 2. Both curves dip to 0 at the space potential.

region during part of the rf cycle, but I_e does not change discontinuously, as it does in the plane case.

Equations (58) and (62) give I_e without the need for solution of Poisson's equation to get $V(r)$. Whether a collisionless electron coming from infinity hits the probe or not depends only on its initial energy and angular momentum regardless of the shape of $V(r)$. The requirement $R_p \ll \lambda_D$ stems from the fact that n has to be small enough that there is no absorption radius R_a inside of which all electrons are collected, thus increasing the effective probe radius from R_p to R_a. To calculate C_{sh}, however, equation (21) requires a knowledge of $\eta(\rho)$, which is not available from the OML theory. Note, however, that the solution given by equations (58) and (62) is self-similar; the only scalelength is given by R_p. The ratio I_e / R_p depends only on η. Thus, as R_p changes, the picture is the same, and only the scale changes. All the particle trajectories have the same shape, and therefore the surface charge density ρ_s is proportional to I_e/R_p, and hence to $F(\eta)$. Let

$$\rho_s = \tau_1 (I_e/A_p), \tag{63}$$

where τ_1 is a constant with the dimensions of time. Equations (20), (58) and (63) then give

$$\frac{C_{sh}}{A_p} = \frac{d\rho_s}{dV} = -\frac{e}{KT_e}\frac{d}{d\eta}(\tau_1 n_0 e v_r F)\,. \tag{64}$$

With equations (9) and (34), this can be written as

$$\frac{C_{sh}}{A_p} = -\frac{1}{\sqrt{2\pi}}\frac{\varepsilon_0}{\lambda_D}\omega_p \tau_1 F'(\eta). \tag{65}$$

Differentiating equation (62) gives

$$F'(\eta) = -e^{-\eta}\{1 - \mathrm{erf}[(-\eta)^{\frac{1}{2}}]\}, \tag{66}$$

where η is negative. The sheath capacitance in electron saturation is therefore

$$\frac{C_{sh}}{A_p} = \frac{1}{\sqrt{2\pi}}\frac{\varepsilon_0}{\lambda_D}\omega_p \tau_1 e^{-\eta}\{1 - \mathrm{erf}[(-\eta)^{\frac{1}{2}}]\}. \tag{67}$$

One might think that the unknown constant τ_1 can be evaluated by matching smoothly to the solution for $\eta > 0$, but this is not the case. In the limit $\eta \to 0$,

$$\frac{C_{sh}}{A_p} = \frac{1}{\sqrt{2\pi}}\frac{\varepsilon_0}{\lambda_D}\omega_p \tau_1 \neq 0, \tag{68}$$

whereas C_{sh} at the space potential has to vanish because there is no sheath. Actually, C_{sh} has to drop to zero even from the electron saturation side. If T_i is finite, though very small, it begins to be collected when $-\eta$ is small, and equation (67) is no longer valid. C_{sh} will fall to zero as in figure 2 but much more steeply, in a voltage range scaled to T_i rather then T_e. Although the absolute magnitude of C_{sh} is not known, we can show its behaviour according to equation (67) in figure 11. There is still a discontinuity at $\eta = 0$, but it is so spiky that it will not be seen, and C_{sh} will vary much more smoothly than in figure 5 when V_{rf} brings η into the electron saturation region.

The statement that the sheath vanishes at $V_p = V_s$ does not hold when there is a dc magnetic field. The probe then casts a shadow, and particles are depleted from the tube of force intercepted by the probe. The space potential inside the tube is different from that outside, and it varies in a way that depends on the diffusion, classical or anomalous, of electrons across the B-field into the tube. Since V_p cannot be V_s everywhere, there is always going to be a sheath, and C_{sh} cannot vanish as it does for an infinitesimal probe in a B-field-free plasma.

A solution for C_{sh} in the Child–Langmuir approximation for cylinders ($\eta \gg 1$) is also available [18], but the series solution is quite cumbersome. For emission from a thin wire out to a sheath edge, Langmuir [18] showed that the solution is insensitive to s/r for $s/r > 10$. This may not be true for ion emission from the outer cylinder rather than the inner one. In any case this C–L solution cannot be connected to the electron retardation region without numerical integration.

6. Conclusion

Both the real and imaginary parts of the sheath impedance of a Langmuir probe vary nonlinearly with rf fluctuations in space potential. An equation for the time-dependent sheath capacitance in plane geometry is derived including both the Child–Langmuir and Debye sheaths. Inclusion of the Debye sheath leads to violent oscillations of the sheath capacitance

which may lead to generation of many harmonics of the rf frequency. For a cylindrical probe the sheath capacitance is given for the electron saturation region, but the transition region requires numerical integration. The effect of rf on probe characteristics can be minimized with an appropriate compensation circuit, whose parameters are specified.

Acknowledgment

This work was partially supported by the National Science Foundation Grant No DMI-0115570.

References

[1] Lieberman M A 1988 *IEEE Trans. Plasma Sci.* **16** 638
[2] Lieberman M A 1989 *IEEE Trans. Plasma Sci.* **17** 338
[3] Godyak V A and Sternberg N 1991 *Proc. 20th Int. Conf. on Phenomena in Ionized Gases (Barga, Italy, July 8–12, 1991)* p 661
[4] Godyak V A and Sternberg N 1990 *Phys. Rev.* A **42** 2299
[5] Zhang Y, Liu J, Liu Y, and Wang X 2004 *Phys. Plasmas* **11** 3840
[6] Sudit I D and Chen F F 1994 *Plasma Sources Sci. Technol.* **3** 162
[7] Godyak V A and Piejak R B 1990 *J. Appl. Phys.* **68** 3157
[8] Gagné R R J and Cantin A 1972 *J. Appl. Phys.* **43** 2639
[9] Cantin A and Gagné R R J 1977 *Appl. Phys. Lett.* **30** 316
[10] Godyak V A, Piejak R B and Alexandrovich B M 1992 *Plasma Sources Sci. Technol.* **1** 36
[11] Mahony C M O, Maguire P D and Graham W G 2005 *Plasma Sources Sci. Technol.* **14** S60
[12] Chen F F 1965 *Plasma Phys.* **7** 47
[13] Allen J E, Boyd R L F and Reynolds P 1957 *Proc. Phys. Soc. (Lond.)* B **70** 297
[14] Chen F F and Arnush D 2001 *Phys. Plasmas* **8** 5051
[15] Laframboise J G 1966 *University of Toronto Institute of Aerospace Studies Report No 100*, National Technical Information Service Document No. AD634596
[16] Mott-Smith H M and Langmuir I 1926 *Phys. Rev.* **28** 727
[17] Chen F F 1965 Electric probes *Plasma Diagnostic Techniques* ed R H Huddlestone and S L Leonard (New York: Academic) Chapter 4, pp 128–35
[18] Langmuir I 1913 *Phys. Rev.* **2** 450